# Cosmochemistry

Bruce Fegley, Jr. and Laura Schaefer

Planetary Chemistry Laboratory, Department of Earth and Planetary Sciences

Washington University

St. Louis, MO 63130-4899

Phone: (314) 935-4852

FAX: (314) 935 -7361

bfegley@wustl.edu

laura_s@wustl.edu

Keywords: cosmochemistry, condensation calculations, elements, solar nebula

## 1 Introduction

Cosmochemistry is the chemistry of the cosmos. This is a broad topic that ranges from the nucleosynthesis of elements in stars to their chemistry on the Earth today. In this chapter, we describe chemical equilibrium (or condensation) calculations of the cosmochemical behavior of the elements.

## 2 Computational Methods

Chemical equilibrium calculations predict the distribution of each element between its gaseous, solid, and liquid compounds as a function of temperature, pressure, and bulk elemental composition. These calculations are often called condensation calculations because they show the stable phases that condense out of a cooling gas with solar system elemental abundances. However, chemical equilibrium calculations are path independent because the Gibbs energy is a state function, i.e., its differential d$G$ is an exact (or perfect) differential. Thus, the results of chemical equilibrium calculations apply equally well to heating or cooling of a solar composition system.

The inputs to the chemical equilibrium calculations are the temperature, pressure, bulk elemental composition, and thermodynamic data for all compounds included in the calculations. The temperatures and pressures used in the calculations depend on the system being studied, e.g., a protoplanetary accretion disk, the photospheric region of a cool star, the ejecta from a nova or supernova, a planetary atmosphere, and so on. The bulk elemental composition is the set of elemental abundances that are appropriate for the system being studied. For example, solar elemental abundances are used for a protoplanetary accretion disk around a solar metallicity star. On the other hand, chemical

equilibrium calculations for the atmospheres of cool carbon stars use bulk compositions that are richer in C, N, and s-process elements than solar abundances [1].

The thermodynamic data for each compound are either the standard Gibbs energy $\Delta G^o$ or equilibrium constant $K_{eq}$ for forming the compound from its constituent elements in their reference states. The reference states are generally the stable form of an element at the ambient temperature. For example, the reaction

$$2H_2\ (gas) + O_2\ (gas) = 2H_2O\ (gas) \qquad (1)$$

forms water vapor from its constituent elements. A second example is the reaction

$$4Al\ (metal) + 3O_2\ (gas) = 2Al_2O_3\ (corundum) \qquad (2)$$

This forms $Al_2O_3$, which is the mineral corundum. The reference state of Al is metal below its melting point, liquid Al from the melting point (933.6 K) to the boiling point (2,798 K), and Al gas at higher temperatures. The coexisting phases at the transition points (i.e., solid and liquid at the melting point or liquid and gas at the boiling point) are in equilibrium with one another, and either can be used as the reference state for aluminum.

The standard Gibbs energy for the formation of water vapor, corundum, or any other compound, from its constituent elements is calculated from tabular data in literature compilations using polynomial equations. The equilibrium constant is related to the $\Delta G^o$ of a reaction by the equation

$$\Delta G^o = -RT\ln K_{eq} \qquad (3)$$

The thermodynamic data come from a number of literature compilations and from primary articles in the scientific literature. Fegley and Lodders [2] list the data sources for

a large number of compounds. Lodders [3, 4] published some updates to this list. The other updates that have been made will be described in future publications.

The chemical equilibrium calculations are done by sophisticated computer codes, such as the CONDOR code [2]. This code simultaneously considers the dual constraints of mass balance and chemical equilibrium. The operation of the CONDOR code and the general principles of chemical equilibrium calculations are best illustrated using a simplified version of iron chemistry in solar composition material.

We define the total elemental abundance of iron as A(Fe). This is the atomic abundance of Fe relative to $10^6$ Si atoms and is 838,000 Fe atoms [5]. The mole fraction ($X$) of total iron (ΣFe) in all Fe-bearing compounds is

$$X_{\sum Fe} = \frac{A(Fe)}{A(H + H_2 + He)} \tag{4}$$

The term $A(H+H_2+He)$ is the sum of the H and He abundances with the temperature-dependent H and $H_2$ equilibrium taken into account. Molecular $H_2$, H, and He are the three major gases in solar composition material over most temperatures and pressures where chemical compounds exist. In the actual computation, other gases such as $H^+$, CO, $H_2O$, $N_2$, Ne, other ions, etc., are also included in the denominator; however, these are neglected in the description here for clarity. Multiplying $X_{\Sigma Fe}$ by the total pressure $P_{\text{tot}}$ gives the partial pressure sum for iron

$$P_{\sum Fe} = X_{\sum Fe} P_T = P_{Fe} + P_{FeS} + P_{FeH} + P_{FeO} \ldots \tag{5}$$

Equation (5) is a mass balance equation that counts the total number of iron atoms in all Fe-bearing gases and equates this sum to the total amount of iron. The partial pressures of

Fe-bearing gases with more than one iron atom are multiplied by the number of iron atoms in the gas to insure that all atoms are counted. In this example the Fe-bearing gases included in the mass balance equation are the most abundant ones at low pressures characteristic of cool stellar atmospheres, protoplanetary disks, and ejecta from nova and supernova. All of these Fe-bearing gases contain one Fe atom and their partial pressures are multiplied by unity. If any gases containing two Fe atoms, such as $Fe_2Cl_4$, were present, their partial pressures would be multiplied by two. We must now relate the partial pressures of the different Fe-bearing gases in the mass balance equation to their chemical equilibrium abundances.

This is done by rewriting equation (5) in terms of the thermodynamic activity of Fe ($a_{Fe}$), the equilibrium constants ($K_i$) for forming the Fe-bearing gases from the constituent elements in their reference states, and the thermodynamic activities and fugacities of all other elements combined with iron in the gases.

$$P_{\sum Fe} = X_{\Sigma Fe} P_T = a_{Fe}[K_{Fe} + K_{FeS} f_{S_2}^{1/2} + K_{FeH} f_{H_2}^{1/2} + K_{FeO} f_{O_2}^{1/2}] \quad (6)$$

The actual mass balance sum for iron in the CONDOR code includes about 21 Fe-bearing gases. The most important ones in a low-pressure, solar composition gas are Fe, FeS, FeH, and FeO. Analogous forms of equation (6) are written for each element in the code. The $a_i$ and $f_i$ terms in equation (6) are the elemental activities and fugacities of the respective elements, e.g., $f_{H2}$ is the fugacity of hydrogen.

Equation (6) combines the mass balance and chemical equilibrium constraints for iron. It also shows that the chemistry of iron is coupled to that of other elements because the fugacities of sulfur, hydrogen, and oxygen are included in equation (6). In general, the

chemistry of all the elements is coupled, and the mass balance equations form a set of coupled, nonlinear equations that are solved iteratively. An initial guess is assumed for the activity or fugacity of each element. These guesses can be optimized if the major gas for each element is known, but this is not necessary for the code to operate properly. The CONDOR code solves the set of mass balance equations and returns the thermodynamic activity or fugacity for each element, the abundances of all gases (molecules, radicals, atoms, and ions) included in the code, and information on the quality of the calculated results for each element. The convergence criterion requires that the calculated and input abundances for each element agree to within 1 part in $10^{15}$. However, for all practical purposes a satisfactory solution is reached when the calculated and input abundances for each element agree to within 1 part in 10,000 (0.01%). At present the CONDOR code considers over 3,600 solid, liquid, and gaseous compounds for all naturally occurring elements in the periodic table.

The CONDOR code also takes possible condensates (both solid and liquid) into account. For example, Fe metal (or liquid Fe depending on the temperature) forms if the thermodynamic activity of Fe ($a_{Fe}$) is equal to or greater than unity. The code computes the temperature at which $a_{Fe}$ reaches unity (the Fe metal condensation temperature), resets $a_{Fe}$ to unity at all temperatures below this point, and adds a new term for the abundance of Fe metal to the mass balance equation.

The stabilities of condensates containing two or more elements are computed considering compound formation from the elements in their respective reference states. For example, the reaction

$$\text{Fe (metal)} + \text{S (ref state)} = \text{FeS (troilite)} \quad (7)$$

is used for troilite, which is the most common Fe sulfide in meteorites. The reference state of sulfur is solid orthorhombic sulfur, solid monoclinic sulfur, liquid sulfur, or $S_2$ gas depending on the temperature. As temperature decreases, reaction (7) shifts to the right and the thermodynamic activity of troilite increases. Troilite condenses when its thermodynamic activity reaches unity and this is calculated from

$$a_{FeS} = a_{Fe} a_S K_{FeS} \quad (8)$$

where $K_{FeS}$ is the temperature-dependent equilibrium constant for troilite formation from its constituent elements, and $a_{Fe}$ and $a_S$ are taken from the gas-phase equilibrium calculations described above. In general, a pure phase such as Fe-metal, corundum ($Al_2O_3$), or troilite (FeS) starts to condense from the gas at the temperature where its thermodynamic activity reaches unity. The thermodynamic activity is less than unity at higher temperatures where the condensate phase is unstable, and is fixed at unity at all temperatures where the condensate is stable.

Once troilite is stable, the fraction of Fe ($\alpha_{Fe}$) condensed in troilite is calculated and the gas-phase abundance of total iron ($P_{Fe}$) is reduced by multiplying by ($1 - \alpha_{Fe}$). Analogous corrections are made for all elements distributed between the gas and condensates. The gas-phase and gas-solid chemical equilibria are coupled and solved simultaneously using iterative techniques. Palme and Fegley [6] illustrate this procedure for condensation of the minerals enstatite $MgSiO_3$ and forsterite $Mg_2SiO_4$, which involve coupled equilibria for the elements Mg, O, and Si.

The total abundance of each condensate is limited by the abundance of the least abundant element in the condensate. For example, the mineral schreibersite $Fe_3P$ forms by reaction of P-bearing gases with Fe metal at about 1300 K and $10^{-4}$ bar total pressure. Phosphorus has an atomic abundance of 8,373 atoms, which is about 1% of the atomic abundance of iron. There are 3 Fe atoms in each molecule of schreibersite. Thus $Fe_3P$ formation consumes only 3% of the total iron abundance, while removing all phosphorus from the gas phase. Likewise, troilite formation removes all sulfur from the gas because its abundance is only 53% of that of iron, while unreacted Fe metal remains present at lower temperatures until it is consumed by formation of Fe-bearing oxides and silicates.

Several points are worth emphasizing. The first point is mass balance. The total amount of each element is conserved in the chemical equilibrium calculations. Thus the abundances of all gases and all condensed phases (solids and/or liquids) sum to the total elemental abundance – no less and no more. The second point is that chemical equilibrium is completely independent of the size, shape, and state of aggregation of condensed phases – a point demonstrated by Willard Gibbs over 130 years ago. Finally, the third point is that chemical equilibrium is path independent. Thus, the results of chemical equilibrium calculations are independent of any particular reaction. A particular chemical reaction does not need to be specified because all possible reactions give the same result at chemical equilibrium. This is completely different than chemical kinetic models where the results of the model are critically dependent on the reactions that are included. However, a chemical equilibrium calculation does not depend on kinetics, is

independent of kinetics, and does not need a particular list of reactions. This point may seem obvious, but is often misunderstood.

## 3 Cosmochemical Behaviors of the Elements

This section summarizes the results of chemical equilibrium calculations for naturally occurring elements. We review the cosmochemical behavior of the elements in order of increasing volatility, i.e., decreasing condensation temperature using the cosmochemical classification scheme.

### 3.1 Refractory Elements

Refractory elements are the first elements to condense (or the last ones to evaporate) from solar composition material. The refractory elements are subdivided into refractory siderophiles (elements found in metal) and refractory lithophiles (elements found as oxides and/or silicates). The refractory siderophiles are the noble or platinum group metals (Ru, Os, Rh, Ir, and Pt, but not Pd), molybdenum Mo, tungsten W, and rhenium Re. All of the refractory siderophiles are trace elements with low abundances. In the 1970s micron-size metal nuggets composed of the refractory siderophile elements were discovered inside Ca, Al-rich inclusions (CAIs) in the Allende meteorite. This is a stony meteorite, which is a type CV3 carbonaceous chondrite. The compositions of the refractory metal nuggets in Allende and other carbonaceous chondrites are reproduced by chemical equilibrium calculations [7, 8].

The actinides (U, Th, Pu), alkaline earths (Be, Mg, Ca, Sr, Ba), lanthanides (elements La – Lu), Al, and the elements in groups 3b (Sc, Y), 4b (Ti, Zr, Hf), and 5b (V, Nb, Ta) of the periodic table are refractory lithophile elements. The refractory lithophiles

are 5% of the total mass of the rock in solar composition material. Aluminum Al, calcium Ca, and titanium Ti are the three most abundant refractory lithophiles, and they form minerals that are the host phases for most of the less abundant refractory lithophile elements such as the actinides, lanthanides, and transition elements in group 5b of the periodic table. Some of the less abundant refractory lithophiles – the group 4b elements Zr, Hf, and the group 3b elements Y and Sc – condense as oxides before any Ca, Al, Ti-bearing minerals form [9]. But the rest condense into the more abundant host phases.

Figure 1 shows the percentage distribution of aluminum between its major gases and the condensed phases that are stable at chemical equilibrium in a solar composition gas as a function of temperature at a total pressure of $10^{-4}$ bar. This pressure is representative of that in the inner regions of protoplanetary accretion disks (such as the solar nebula) and photospheric regions of cool stars.

At the high temperatures that are shown on the right hand side of Figure 1, all Al is in the gas phase, mainly as monatomic Al and aluminum hydroxide AlOH gases. For example at 2000 K, about 92% of all aluminum is in Al gas, about 7.5% is in AlOH gas, and the remaining 0.5% is in other Al-bearing gases. Corundum $Al_2O_3$ condenses at 1640 K and is the first Al-bearing mineral (see the small wedge at the top right of Figure 1). However, Figure 1 shows that corundum is only stable for a few degrees (the wedge disappears). Grossite $CaAl_4O_7$ and hibonite $CaAl_{12}O_{19}$ form by reaction of corundum with the surrounding gas. These reactions destroy all the corundum and produce grossite and hibonite. At 1600 K, most of the Al is in these minerals. The remainder is mainly in gaseous AlOH and Al. In fact, Figure 2 shows that other Al-bearing gases are still present

but that these are less abundant than Al or AlOH. In turn, other reactions form the mineral gehlenite $CaAl_2SiO_7$ from grossite and hibonite with decreasing temperature. The rest of Figure 1 shows the appearance, disappearance, and abundance of other Al-bearing condensates formed at chemical equilibrium at lower temperatures.

Figure 2 shows the mole fractions of the major Al-bearing gases that are stable at chemical equilibrium in a solar composition gas as a function of temperature at a total pressure of $10^{-4}$ bar. The temperature range in Figure 2 is only from 1200 – 2000 K because the mole fractions of all the Al-bearing gases decrease strongly with decreasing temperature below the condensation temperature of corundum. Figures 1 and 2 are complementary to one another. Figure 1 gives the percentage distribution relative to total aluminum while Figure 2 gives the mole fractions, defined as the partial pressure of a gas relative to the total pressure. For example, the mole fraction of AlOH gas is

$$X_{AlOH} = \frac{P_{AlOH}}{P_T} \tag{9}$$

This definition of mole fraction is identical to saying that the mole fraction is equal to the number of moles of a gas relative to the moles of all gases, or equivalently that the mole fraction of a gas is equal to its volume fraction. Figure 2, and similar figures for other elements, show gases that are not abundant enough to appear on a percentage distribution graph such as Figure 1. This information is important for astronomical observations of the photospheric regions of cool stars, of protoplanetary accretion disks, of circumstellar envelopes, and of the atmospheres of gas giant planets.

Table 1 lists the names and formulas of the minerals shown in Figure 1 and subsequent figures. For example, Table 1 shows that the mineral grossite has the formula

$CaAl_4O_7$ and that $MgAl_2O_4$ is the mineral spinel. Table 2 lists the elements discussed in this chapter in decreasing order of abundance. Table 2 also gives the major gases and initial condensates of these elements. For example, Table 2 shows that Al is the twelfth most abundant element in solar composition material with an abundance of $8.41 \times 10^4$ Al atoms (per $10^6$ Si atoms), its initial condensates are corundum $Al_2O_3$ at 1640 K and hibonite $CaAl_{12}O_{19}$ at 1620 K, and its major gases are Al and AlOH.

Figures 3 and 4 for Ca and Ti, respectively, give similar information for the major gases and condensates of these two refractory lithophiles. For example, monatomic Ca gas is the major Ca-bearing gas and hibonite $CaAl_{12}O_{19}$ is the first Ca-bearing condensate. Likewise, titanium monoxide TiO, $TiO_2$, and monatomic Ti are the major Ti-bearing gases and perovskite $CaTiO_3$ is the first Ti-bearing condensate.

The results of the chemical equilibrium calculations for the refractory lithophiles are also confirmed by the mineralogy and chemistry of the Ca, Al-rich inclusions in Allende and other meteorites. The major minerals in CAIs are the same ones predicted by the calculations, namely melilite (a solid solution of gehlenite $CaAl_2SiO_7$ and åkermanite $Ca_2MgSi_2O_7$), spinel, corundum, grossite, hibonite, and perovskite. Chemical analyses of CAIs show that the refractory lithophiles are enriched by an average of 20 times solar elemental abundances, as expected for complete condensation of elements that constitute 5% of rocky material. The less abundant refractory lithophiles, such as the lanthanides (or rare earth elements REE) are found dissolved in perovskite and hibonite, as predicted by chemical equilibrium calculations. Kornacki and Fegley [9, 10] describe chemical equilibrium calculations for refractory lithophiles and their abundances in CAIs.

### 3.2 Major elements

Iron Fe, magnesium Mg, and silicon Si are the next elements to condense and they constitute the major elements because they make up most of the rock in solar composition material. Figure 5 shows the percentage distribution of iron between its major gases and condensates. Iron metal condenses at 1357 K at $10^{-4}$ bar total pressure and is 50% condensed by 1325 K. The iron metal is not pure Fe, but is an Fe-rich metal alloy containing smaller amounts of nickel Ni, cobalt Co, and other siderophile elements. Iron metal is the only Fe-bearing condensate until schreibersite $Fe_3P$ forms (1285 K, $10^{-4}$ bars). As mentioned earlier, phosphorus is about 1% as abundant as Fe, so formation of $Fe_3P$ consumes only 3% of the total iron metal. The formation of troilite FeS at 704 K consumes about 55% of the remaining Fe metal. Hydrogen sulfide is the major S-bearing gas containing about 100% of all sulfur and troilite formation occurs via the net thermochemical reaction

$$H_2S\ (gas) + Fe\ (metal) = FeS\ (troilite) + H_2\ (gas) \qquad (10)$$

This reaction has the same number of gas molecules on either side of the reaction and the FeS formation temperature of 704 K is thus independent of total pressure.

Chromite $FeCr_2O_4$ formation at 660 K consumes a tiny fraction of Fe metal, but the remainder of the metal remains present until it is oxidized to $Fe^{2+}$-bearing silicates such as fayalite $Fe_2SiO_4$, shown in Figure 5. This dissolves in solid solution with forsterite $Mg_2SiO_4$ forming olivine.

Figures 6 and 7 show the equilibrium chemistry of magnesium and silicon. Small amounts of magnesium and silicon condense at high temperatures as spinel $MgAl_2O_4$

(1390 K, shown in Figure 1), gehlenite $Ca_2Al_2SiO_7$ (1529 K), and åkermanite $Ca_2MgSi_2O_7$ (not shown). However the amounts of Mg and Si in these high temperature condensates are limited by Ca and Al, which are much less abundant than magnesium or silicon. Most Mg and Si condense as forsterite $Mg_2SiO_4$ (1354 K) and enstatite $MgSiO_3$ (1290 K). Forsterite condenses from the gas phase while enstatite forms by reaction of nebular gas with preexisting forsterite grains.

Figure 8 shows that at pressures greater than about $10^{-4}$ bar, Fe metal condenses at higher temperatures than forsterite $Mg_2SiO_4$. Conversely, at pressures less than about $10^{-4}$ bar, forsterite condenses at higher temperatures than Fe metal. The separation between the metal and forsterite condensation temperatures increases with increasing pressure from the crossover point. The planet Mercury is richer in Fe and poorer in silicates than expected from solar composition. This may indicate that the materials accreted by Mercury formed at pressures higher than the $10^{-4}$ bar crossover point for the iron and forsterite condensation curves.

**3.3 Moderately Volatile Elements**

The moderately volatile elements are the next elements to condense from cooling solar composition material. The moderately volatile elements are a diverse set of elements including the alkali elements (Li, Na, K, Rb, Cs); transition metals (Cr, Co, Mn, Ni, Pd, Cu, Ag, Au, Zn); group 3 elements (B and Ga); group 4 elements (Ge and Sn); group 5 elements (P, As, Sb); group 6 elements (S, Se, Te); and two of the halogens (F and Cl). Moderately volatile elements have condensation temperatures between those of the major elements (Fe, Mg, Si) and troilite FeS. The moderately volatile elements with

higher abundances condense as pure phases. For example, Figures 5 and 9 show that sulfur condenses as troilite FeS at 704 K. As mentioned above, $H_2S$ is the dominant S-bearing gas at the troilite condensation temperature. Figure 9 shows that S, SH, and SiS are important and that PS and $S_2$ are minor S-bearing gases at higher temperatures. However, these gases are highly reactive and cannot survive at lower temperatures. For example, the condensation of forsterite $Mg_2SiO_4$ and enstatite $MgSiO_3$ removes all silicon, including SiS, from the gas. Condensation of schreibersite $Fe_3P$ removes PS and all other P-bearing gases. Finally, monatomic S, SH, and $S_2$ convert into $H_2S$ with decreasing temperature.

Figures 5 and 10 show that phosphorus condenses as schreibersite $Fe_3P$ at 1285 K. Schreibersite reacts with nebular gas at lower temperatures and forms fluorapatite $Ca_5(PO_4)_3F$ at 710 K and whitlockite $Ca_3(PO_4)_2$ at 680 K. The whitlockite reacts with HCl in the nebular gas to form chlorapatite $Ca_5(PO_4)_3Cl$ at 470 K. Chondrites contain all these phosphate minerals. Figures 11 and 12 show the equilibrium chemistry of fluorine and chlorine, which illustrate an interesting mass balance example. Fluorine is the least abundant element in fluorapatite and its abundance limits that of fluorapatite. The 3:1 ratio of P to F atoms in fluorapatite consumes about 30% of total phosphorus, leaving 70% of total phosphorus for chlorapatite formation. However, this is not enough to condense all chlorine, which requires a 3:1 ratio of P to Cl atoms to condense all chlorine in chlorapatite. In fact, the total phosphorus abundance is too small to condense all Cl in chlorapatite. The residual chlorine, which is about 60% of total Cl, condenses as halite NaCl (420 K). However, this forms sodalite $Na_4(AlSiO_4)_3Cl$ (405 K, and again at 315 K),

which decomposes back to halite plus nepheline (365 K), over the 405 – 315 K range. Both minerals are found in chondrites. Halite is probably present in many chondrites that contain water-soluble chlorine, even though it is not reported as one of the observed minerals.

Sodium and potassium condense initially as the feldspar minerals albite $NaAlSi_3O_8$ and orthoclase $KAlSi_3O_8$. Some of the albite reacts to form halite at 420 K. Formation of glaucophane, a hydrous mineral called an amphibole, consumes the remaining albite at 360 K. Likewise, formation of phlogopite, a hydrous mineral called a mica, consumes all orthoclase at 470 K. Neither glaucophane nor phlogopite occurs in meteorites. Thus, although they become thermodynamically stable at low temperatures, they may not form because of slow chemical reaction rates.

Most of the moderately volatile elements have low abundances and condense in solid solutions in more abundant minerals. For example, selenium Se may dissolve in FeS as FeSe. Copper, Ag, and Au may dissolve in Fe alloy. Lithium, Mn, and Zn condense into forsterite and enstatite, e.g. as $LiSiO_3$, $Mn_2SiO_4$, $MnSiO_3$, $Zn_2SiO_4$, and $ZnSiO_3$. Boron and gallium substitute for Al in feldspar and Rb and Cs substitute for K in orthoclase. Some elements such as gallium are found in metal and silicates in meteorites, and gallium may dissolve in both phases during condensation.

### 3.4 Highly Volatile Elements

The highly volatile elements (Bi, Br, Cd, Hg, I, In, Pb, Tl) condense at temperatures between troilite and water ice. In general, the equilibrium chemistry of these elements is poorly known because thermodynamic data are unavailable for some pure

phases and solid solutions. Most of the highly volatile elements condense in solid solution in more abundant minerals. For example, Lodders [5] calculated that mercury condenses as HgS, HgSe, and HgTe dissolved in solid solution in troilite FeS. Fifty percent of all Hg is condensed at 252 K. Her result predicts that the CI carbonaceous chondrites should contain the solar abundance of mercury. At present, the Hg solar abundance is estimated from r-process and s-process systematics of the elements. Bismuth Bi, and lead Pb condense in solid solution in iron metal alloy, while cadmium, In, and Tl condense in solid solution in troilite FeS. Bromine and iodine condense in solid solution in the apatite minerals. Lodders [5] gives a good discussion of condensation chemistry of the moderately and highly volatile elements in solar composition material.

**3.5 Atmophile Elements**

The atmophile elements (H, C, N, noble gases) condense at and below the condensation temperature of water (liquid or ice). Liquid water or water ice condenses at the temperature where the partial pressure of water vapor equals the vapor pressure over liquid water or water ice. The condensation curve for water (liquid or ice) is

$$\frac{10{,}000}{T_C(H_2O)} = 38.84 - 3.83 \log_{10} P_T \qquad (11)$$

Thus, water ice starts to condense at 185 K at $10^{-4}$ bars total pressure in solar composition material. Fifty percent of all water condenses by 180 K. Liquid water condenses instead of water ice at total pressures of ~ 3.8 bars and above. Condensation of liquid water has important consequences such as the formation of aqueous $NH_3$ solutions. Aqueous $NH_3$ solutions are stable down to 173 K at one bar total pressure, which is the eutectic point, i.e., the lowest melting point, in the $NH_3 - H_2O$ phase diagram [11].

The partial pressure of water vapor in solar composition material depends on several factors. Formation of anhydrous minerals consumes about 23% of total oxygen. The formation of hydrous minerals, such as glaucophane, tremolite, serpentine, and talc consumes more water vapor. For example, serpentine and brucite $Mg(OH)_2$ form by the hydration of forsterite $Mg_2SiO_4$ grains by water vapor

$$2Mg_2SiO_4 \text{ (forsterite)} + 3H_2O \text{ (g)} = Mg_3Si_2O_5(OH)_4 \text{ (serpentine)} + Mg(OH)_2 \text{ (brucite)} \quad (12)$$

An analogous reaction is formation of talc and brucite by hydration of enstatite grains

$$4MgSiO_3 \text{ (enstatite)} + 2H_2O \text{ (g)} = Mg_3Si_4O_{10}(OH)_2 \text{ (talc)} + Mg(OH)_2 \text{ (brucite)} \quad (13)$$

These hydration reactions provide hydrous minerals at low temperatures in solar composition material (~250 K for serpentine and ~300 K for talc). By mass, serpentine contains 13.0% water, talc 4.8% water, and brucite 3.1% water. Theoretical models of gas – grain kinetics predict that hydration of forsterite and enstatite to serpentine and talc are too slow to proceed over the lifetime of the solar nebula [12]. These predictions are consistent with petrological studies of meteorites containing hydrous silicates, which conclude that hydrous minerals formed on the meteorite parent bodies.

The partitioning of carbon between CO and $CH_4$ also affects the water vapor partial pressure. As discussed below, CO is the major C-bearing gas at high temperatures and low pressures while $CH_4$ is the major C-bearing gas at low temperatures and high pressures. Because the bulk C/O ratio is 0.5 in solar composition material, the water vapor abundance increases by about a factor of two when CO converts to methane. All these factors are summarized in Figure 13, which shows the percentage distribution of oxygen between the major O-bearing gases and minerals. At complete chemical

equilibrium, the anhydrous and hydrous minerals consume about 26% of all oxygen and about 74% is left to condense as water or water ice.

The condensation chemistry of carbon and nitrogen depends on the major C- and N-bearing gases at low temperatures in solar composition material. At $10^{-4}$ bar total pressure, $CH_4$ and $NH_3$ are the predominant C- and N-bearing gases at temperatures below the water ice (or liquid water) condensation curve. Ammonia condenses as ammonia monohydrate $NH_3 \cdot H_2O$ at 131 K, $10^{-4}$ bars total pressure via the net reaction

$$NH_3\ (g) + H_2O\ (ice) = NH_3 \cdot H_2O\ (ice) \qquad (14)$$

Ammonia monohydrate (also called ammonium hydroxide $NH_4OH$) is a distinct compound and is not a clathrate hydrate. Ammonia ice and/or liquid $NH_3$ could form in the absence of liquid water. This happens in Jupiter's atmosphere where $NH_3$ ice clouds form because gravitational sedimentation keeps liquid water droplets in a cloud layer hundreds of kilometers below the $NH_3$ ice clouds. Thus, no water is present in the upper atmosphere where the $NH_3$ ice clouds form. Liquid $NH_3$ does not condense in the solar nebula or on the gas giant planets in our solar system (Jupiter, Saturn, Uranus, and Neptune) because the total pressure and/or $NH_3$ gas abundance is too low. The $NH_3$ gas pressure would have to be at least as high as the triple point pressure (0.06 bars at 195.5 K) for liquid $NH_3$ condensation. Assuming that all nitrogen is present as $NH_3$, the total pressure at low temperatures would have to be about 444 bars for liquid $NH_3$ to form (i.e., to reach 0.06 bars $NH_3$ pressure at the triple point) in solar composition material. Such high pressures are unreasonable for the solar nebula but they may occur in extrasolar gas giant planets or in the interiors of icy planets and satellites.

Methane condenses at lower temperatures as methane clathrate hydrate ($CH_4 \cdot 7H_2O$) at 78 K and $CH_4$ ice. A clathrate hydrate is a cage compound in which a gas molecule is trapped inside the water ice crystal lattice. One gas atom is trapped for every seven water molecules. Clathrate hydrates form via reactions exemplified by

$$CH_4 \text{ (gas)} + 7H_2O \text{ (ice)} = CH_4 \cdot 7H_2O \text{ (clathrate hydrate)} \quad (15)$$

However, there is not enough water ice to condense all $CH_4$ as a clathrate hydrate because the $CH_4$ to $H_2O$ ratio is 1:7 in the clathrate hydrate while the solar C/O ratio is 0.5. Thus, the residual $CH_4$ condenses as $CH_4$ ice at lower temperatures. Hydrogen and helium do not condense because temperatures never get low enough for solid hydrogen or liquid helium to form. Neon ice forms at about 9 K, but it is doubtful if temperatures ever get this low in any astronomical environment where condensation occurs. The other noble gases (Ar, Kr, Xe) either condense as ices (solid Ar, Kr, Xe) or form clathrate hydrates (Ar 48 K, Kr 53 K, Xe 69 K). The condensation temperatures given for the noble gas clathrate hydrates assume that sufficient water ice is available for reaction and that all of each noble gas forms a clathrate hydrate. If no water ice is available, the noble gases condense as ices at lower temperatures than their clathrates form.

The condensation chemistry of carbon and nitrogen depends on whether or not $CH_4$ and $NH_3$ are the predominant C- and N-bearing gases. The two major C-bearing gases in solar composition material over a wide P, T range are CO and $CH_4$. These two gases are converted into one another by the net reaction

$$CO + 3H_2 = CH_4 + H_2O \quad (16)$$

$$\log K_{16} = 11{,}069.94/T - 1.17969 \log T - 8.96596 \quad (17)$$

Equation (17) gives the equilibrium constant for reaction (16) from 298 – 2500 K. Chemical equilibrium calculations using this data and the solar elemental abundances show that CO is stable at high temperatures and low pressures while $CH_4$ is stable at low temperatures and high pressures in solar composition material (e.g., see [13]). For example, at $10^{-4}$ bar total pressure, CO is the major C-bearing gas at temperatures greater than 625 K, $CH_4$ is the major C-bearing gas at temperatures less than 625 K, and the two gases have equal abundances at 625 K. The equal abundance point shifts to higher temperatures with higher pressures, as shown in Figure 14.

However, the kinetics of the gas phase conversion of CO to $CH_4$ become so slow that it may not happen unless grain catalyzed reactions occur. If all carbon remained as CO at the low temperatures in solar composition material, then the water ice abundance was decreased below the amount which could condense if CO were converted to $CH_4$. On the other hand, if CO were efficiently converted to $CH_4$ and/or other hydrocarbons, then a sizable fraction of the total O was released from CO and was available for formation of water ice. The water ice/rock mass ratios in "icy" bodies formed in the solar nebula, where CO was the dominant carbon gas, are predicted to be lower than the water ice/rock ratios in "icy" bodies formed in the subnebulae around Jupiter and Saturn, where $CH_4$ was the dominant carbon gas. (Planetary scientists think that the Galilean satellites (Io, Europa, Ganymede, and Callisto) of Jupiter and Titan and other regular satellites of Saturn formed in miniature versions of the solar nebula known as subnebulae. These existed around Jupiter and Saturn during their formation and were higher density regions

with different chemistry than the surrounding solar nebula.) To first approximation, this distinction is observed and supports the chemical modeling.

The two major N-bearing gases in solar composition material are $N_2$ and $NH_3$ (see Figure 15). They are converted into one another by the net thermochemical reaction

$$N_2 + 3H_2 = 2NH_3 \tag{18}$$

$$\log K = 6051.59/T - 1.21176 \log T - 7.89739 \tag{19}$$

Equation (19) gives the equilibrium constant from 298 – 2500 K for reaction (18). Chemical equilibrium calculations using this data and the solar elemental abundances show that $N_2$ is the dominant N-bearing gas at high temperatures and low pressures and that $NH_3$ is the major N-bearing gas at low temperatures and high pressures. Figure 15 shows the $N_2/NH_3$ equal abundance line over a wide P, T range. At higher temperatures, $N_2$ is the only nitrogen-bearing gas of any importance. Along the $10^{-4}$ bar isobar, $NH_3$ remains the second most abundant N-bearing gas until about 1670 K where monatomic N becomes the second most abundant gas. However, even at 2000 K, $10^{-4}$ bars the $N_2/N$ molecular ratio is 100,000 and all other N-bearing gases are less abundant.

The $N_2/NH_3$ equal abundance line is slightly different from the $CO/CH_4$ equal abundance line because equal abundances of $N_2$ and $NH_3$ do not correspond to 50% of total nitrogen in each gas. Figure 15 shows that at $10^{-4}$ bars total pressure, $N_2$ and $NH_3$ have equal abundances at 345 K, but 50% of total nitrogen is in each gas at 320 K. At lower temperatures, $NH_3$ first condenses as ammonium carbonate $NH_4HCO_3$, or ammonium carbamate ($NH_4COONH_2$). The exact amount of $NH_3$ in these compounds depends upon the amount of $CO_2$ and is hard to quantify because the amount of $CO_2$

depends on the rate of the CO to $CO_2$ conversion in different astronomical environments such as the solar nebula or another protoplanetary accretion disk. The remaining $NH_3$ condenses as ammonia monohydrate ($NH_3 \cdot H_2O$) at 131 K, $10^{-4}$ bars.

However, the gas phase conversion of $N_2$ to $NH_3$ is a slow reaction and may not occur over long times, such as the lifetime of the solar nebula. Industrial production of $NH_3$ from $N_2$ (the Bosch – Haber process) uses Fe-based catalysts to speed up the reaction. Iron-rich metal grains and magnetite $Fe_3O_4$ grains are common in chondritic meteorites and it is likely that such grains catalyzed the $N_2$ to $NH_3$ conversion in the solar nebula and other solar composition systems, e.g. see [14]. If $N_2$ remains the major N-bearing gas due to kinetic limitations, N-bearing ices do not form until very low temperatures where either $N_2$ clathrate hydrate or $N_2$ ice condense. Temperatures of 20 – 40 K are required for this to happen.

The most important of the atmophile elements is hydrogen, which is the most abundant element in solar composition material. Hydrogen's dominance controls the chemistry of solar composition material. With the exception of helium, which is non-reactive, hydrogen is about 1,000 times as abundant as all other elements combined. Thus, hydrogen-bearing gases (hydrides) are major or important gases at chemical equilibrium for many elements. A few examples are $H_2O$, $CH_4$ (at low temperatures), $NH_3$ (at low temperatures), $H_2S$, HF, HCl, and HBr.

Most hydrogen remains in elemental form because no other element amounts to more than about 0.1% of the hydrogen elemental abundance. Figure 16 illustrates this point. It shows the mole fractions of the major H-bearing gases. By definition, the mole

fractions of all gases that are present add up to unity. Figure 16 shows that the major H-bearing gases are always elemental gases. With decreasing temperature the major H-bearing gas changes from ionized hydrogen $H^+$ (at temperatures higher than those shown on the graph), to monatomic hydrogen H, and finally to molecular hydrogen $H_2$. The hydrides and all other H-bearing gases are much less abundant than the different allotropes of hydrogen.

Figure 17 shows the percentage distribution (on a logarithmic scale) of hydrogen between the major H-bearing gases over the same temperature range. Figure 17 shows that $H_2$ is 50% dissociated to monatomic H at 2,230 K (i.e., the temperature where each gas has a mole fraction of 0.50). Monatomic H is 50% ionized to $H^+$ at 8,700 K, above the highest temperature on the graphs. Thermal ionization of monatomic H occurs via the reaction

$$H\ (gas) = H^+\ (gas) + e^-\ (gas) \qquad (20)$$

The electron pressure in this reaction is that produced by the ionization of *all* elements in a solar composition gas – not only the electron pressure due to hydrogen ionization. As the total pressure decreases, thermal dissociation and ionization of hydrogen become more important at lower temperatures. For example, hydrogen is 50% dissociated at 1,880 K and 50% ionized at 7,100 K at $10^{-6}$ bar total pressure.

**4 Summary**

In this chapter, we reviewed the methods and results of chemical equilibrium calculations applied to solar composition material. These types of calculations are applicable to chemistry in a variety of astronomical environments including the atmospheres and

circumstellar envelopes of cool stars, the solar nebula and protoplanetary accretion disks around other stars, planetary atmospheres, and the atmospheres of brown dwarfs. The results of chemical equilibrium calculations have guided studies of elemental abundances in meteorites and presolar grains and as a result have helped to refine nucleosynthetic models of element formation in stars.

**Acknowledgments**

This work was supported by funding from the NASA Astrobiology Program.

**References**

1. K. Lodders, B. Fegley, Jr.: Condensation Chemistry of Carbon Stars. In: *Astrophysical Implications of the Laboratory Study of Presolar Materials,* AIP Conference Proceedings v. 402, ed by T. J. Bernatowicz, E. Zinner (American Institute of Physics, Woodbury, NY 1997) pp 391-423
2. B. Fegley, Jr., K. Lodders: Icarus **110**, 117 (1994)
3. K. Lodders: J. Phys. Chem. Ref. Data **28**, 1705 (1999)
4. K. Lodders: J. Phys. Chem. Ref. Data **33**, 357 (2004)
5. K. Lodders: Astrophys. J. **591**, 1220 (2003)
6. H. Palme, B. Fegley, Jr.: Earth Planet. Sci. Lett. **101**, 180 (1990)
7. H. Palme, F. Wlotzka: Earth Planet. Sci. Lett. **33**, 45 (1976)
8. B. Fegley, Jr., H. Palme: Earth Planet. Sci. Lett. **72**, 311 (1985)
9. A. S. Kornacki, B. Fegley, Jr.: Earth Planet. Sci. Lett. **79**, 217 (1986)
10. A. S. Kornacki, B. Fegley, Jr.: Proc. 14$^{th}$ Lunar Planet. Sci. Conf. J. Geophys. Res. **89**, B588(1984)
11. J. S. Lewis: Earth Planet. Sci. Lett. **15**, 286 (1972)
12. B. Fegley, Jr.: Trends of Volatile Elements in the Solar System. In: *Workshop on the Origins of Solar Systems* ed by J. A. Nuth, P. Sylvester (LPI, Houston 1988) Tech. Rep. No. 88-04, p. 51.
13. K. Lodders, B. Fegley, Jr.: Icarus **155**, 393 (2002)
14. B. Fegley, Jr., R. G. Prinn: Solar Nebula Chemistry: Implications for Volatiles in the Solar System. In: *The Formation and Evolution of Planetary Systems*, ed by H. Weaver, L. Danly (Cambridge University Press, Cambridge, UK 1989) pp 171-211

**Table 1.** Minerals Included in Figures

| Mineral name | Formula |
|---|---|
| Alabandite | MnS |
| Albite | $NaAlSi_3O_8$ |
| Anorthite | $CaAl_2Si_2O_8$ |
| Bornite | $Cu_5FeS_4$ |
| Chlorapatite | $Ca_5(PO_4)_3Cl$ |
| Chromite | $FeCr_2O_4$ |
| (Cobalt sulfide)[a] | $Co_9S_8$ |
| Corundum | $Al_2O_3$ |
| Diopside | $CaMgSi_2O_6$ |
| Enstatite | $MgSiO_3$ |
| Eskolaite | $Cr_2O_3$ |
| Fayalite | $Fe_2SiO_4$ |
| Fluorapatite | $Ca_5(PO_4)_3F$ |
| Forsterite | $Mg_2SiO_4$ |
| Gehlenite | $Ca_2Al_2SiO_7$ |
| Glaucophane | $Na_2Mg_3Al_2Si_8O_{22}(OH)_2$ |
| Grossite | $CaAl_4O_7$ |
| Halite | NaCl |
| Heazlewoodite | $Ni_3S_2$ |
| Hibonite | $CaAl_{12}O_{19}$ |
| Hydroxyapatite | $Ca_5(PO_4)_3OH$ |
| Ilmenite | $FeTiO_3$ |
| Iron metal | Fe |
| (iron selenide)[a] | $FeSe_{0.961}$ |
| Karelianite | $V_2O_3$ |
| Orthoclase | $KAlSi_3O_8$ |
| Perovskite | $CaTiO_3$ |
| Phlogopite | $KMg_3AlSi_3O_{10}(OH)_2$ |
| Picrochromite | $MgCr_2O_4$ |
| Rutile | $TiO_2$ |
| Schreibersite | $Fe_3P$ |
| Sodalite | $3NaAlSiO_4 \cdot NaCl$ |
| (Sodium bromide)[a] | NaBr |
| Spinel | $MgAl_2O_4$ |
| Talc | $Mg_3Si_4O_{10}(OH)_2$ |
| Tephroite | $Mn_2SiO_4$ |
| (Titanium oxide)[a] | $Ti_4O_7$ |
| Tremolite | $Ca_2Mg_5Si_8O_{22}(OH)_2$ |
| Troilite | FeS |
| Zincochromite | $ZnCr_2O_4$ |

[a] No known mineral name.

**Table 2.** Abundances and Condensation Temperatures of the Elements in the Solar Nebula

| | Element | Symbol. | Abundance | $T_C$ (K) | Initial Condensate {Dissolving Species} | 50% $T_C$ (K) | Major gases |
|---|---|---|---|---|---|---|---|
| 1 | Hydrogen | H | $2.431\times10^{10}$ | 182 | $H_2O$ ice | — | $H_2$ |
| 2 | Helium | He | $2.343\times10^{9}$ | <3 | He ice | — | He |
| 3 | Oxygen | O | $1.413\times10^{7}$ | 182 | $H_2O$ ice[a] | 180 | CO, $H_2O$ |
| 4 | Carbon | C | $7.079\times10^{6}$ | 78 | $CH_4{\cdot}7H_2O$ | 40 | CO, $CH_4$ |
| 5 | Neon | Ne | $2.148\times10^{6}$ | 9.3 | Ne ice | 9.1 | Ne |
| 6 | Nitrogen | N | $1.950\times10^{6}$ | 131 | $NH_3{\cdot}H_2O$ | 123 | $N_2$, $NH_3$ |
| 7 | Magnesium | Mg | $1.020\times10^{6}$ | 1390 | Spinel | — | Mg |
| | | | | 1354 | Forsterite[b] | 1336 | |
| 8 | Silicon | Si | $\equiv1.00\times10^{6}$ | 1529 | Gehlenite | — | SiO,SiS |
| | | | | 1290 | Enstatite | 1265 | |
| 9 | Iron | Fe | $8.380\times10^{5}$ | 1357[c] | Fe metal[c] | 1325 | Fe |
| 10 | Sulfur | S | $4.449\times10^{5}$ | 704 | FeS | 655 | $H_2S$,HS |
| 11 | Argon | Ar | $9.032\times10^{4}$ | 48 | $Ar{\cdot}6H_2O$ | 47 | Ar |
| 12 | Aluminum | Al | $8.410\times10^{4}$ | 1640 | $Al_2O_3$ | 1653 | Al, AlOH, $Al_2O$, AlS, |
| | | | | 1620 | $CaAl_{12}O_{19}$ | 1615 | AlH, AlO |
| 13 | Calcium | Ca | $6.287\times10^{4}$ | 1620 | $CaAl_{12}O_{19}$ | — | Ca |
| | | | | 1529 | Gehlenite | 1500 | |
| 14 | Sodium | Na | $5.751\times10^{4}$ | 970 | $\{NaAlSi_3O_8\}$ | 960 | Na, NaCl |
| 15 | Nickel | Ni | $4.780\times10^{4}$ | 1280 | {Ni} | 1260 | Ni |
| 16 | Chromium | Cr | $1.286\times10^{4}$ | 870 | $Cr_2O_3$ | | Cr |
| 17 | Manganese | Mn | 9168 | 1050 | MnS | — | Mn |
| 18 | Phosphorus | P | 8373 | 1285 | $Fe_3P$ | 1265 | PO, P, PN, PS |
| 19 | Chlorine | Cl | 5237 | 650 | $Ca_5(PO_4)_3Cl$ | — | HCl, NaCl, KCl |
| | | | | — | $Na_4[Al_3Si_3O_{12}]Cl$ | 400 | |
| 20 | Potassium | K | 3692 | 950 | $\{KAlSi_3O_8\}$ | 915 | K, KCl, KOH |
| 21 | Titanium | Ti | 2422 | 1593 | $CaTiO_3$ | 1575 | TiO, $TiO_2$ |

**Table 2.** Abundances and Condensation Temperatures of the Elements in the Solar Nebula

| | Element | Symbol. | Abundance | $T_C$ (K) | Initial Condensate {Dissolving Species} | 50% $T_C$ (K) | Major gases |
|---|---|---|---|---|---|---|---|
| 22 | Cobalt | Co | 2323 | 1190 | {Co} | 1170 | Co |
| 23 | Zinc | Zn | 1226 | 660 | $ZnCr_2O_4$ | 650 | Zn |
| 24 | Fluorine | F | 841.1 | 710 | $Ca_5[PO_4]_3F$ | 710 | HF |
| 25 | Copper | Cu | 527.0 | 960 | {Cu} | 940 | Cu |
| 26 | Vanadium | V | 288.4 | — | $\{VO,V_2O_3\}$ | 1250 | $VO_2$, VO |
| 27 | Selenium | Se | 65.79 | — | ZnSe | 520 | $H_2Se$, GeSe |
| 28 | Krypton | Kr | 55.15 | 53 | $Kr{\cdot}6H_2O$ | 52 | Kr |
| 29 | Bromine | Br | 11.32 | 370 | NaBr | 360 | Br, HBr |

[a]22.75% of oxygen is condensed into rock before water ice condensation. [b]Major condensed reservoir of element.
[c]Condensation temperature of pure iron metal.

Figure Captions

Figure 1. Percentage distribution of aluminum between different phases in a solar composition gas as a function of temperature for a total pressure of $10^{-4}$ bars. Gaseous species are indicated with (g), all other species are condensed phases.

Figure 2. Gas phase chemistry of aluminum in a solar composition gas as a function of temperature at a total pressure of $10^{-4}$ bars. The abundances of the gases are shown as mole fractions.

Figure 3. Percentage distribution of calcium between different phases in a solar composition gas as a function of temperature for a total pressure of $10^{-4}$ bars. Gaseous species are indicated with (g), all other species are condensed phases. Hydroxyapatite ($Ca_5(PO_4)_3OH$) is not shown because it occurs only at 300 K (and lower) with an abundance of 15.5% of total Ca.

Figure 4. Percentage distribution of titanium between different phases in a solar composition gas as a function of temperature for a total pressure of $10^{-4}$ bars. Gaseous species are indicated with (g), all other species are condensed phases.

Figure 5. Percentage distribution of iron between different phases in a solar composition gas as a function of temperature for a total pressure of $10^{-4}$ bars. Gaseous species are indicated with (g), all other species are condensed phases.

Figure 6. Percentage distribution of magnesium between different phases in a solar composition gas as a function of temperature for a total pressure of $10^{-4}$ bars. Gaseous species are indicated with (g), all other species are condensed phases. Spinel ($MgAl_2O_4$)

and talc ($Mg_3Si_4O_{10}(OH)_2$) are not shown due to their low abundance (1.4% and 0.9 % total Mg at 300 K, respectively).

Figure 7. Percentage distribution of silicon between different phases in a solar composition gas as a function of temperature for a total pressure of $10^{-4}$ bars. The abundances of the phases are shown as a cumulative percentage of the element. Gaseous species are indicated with (g), all other species are condensed phases. Not shown due to low abundance: $KMg_3AlSi_3O_{10}(OH)_2$ (1.1 %), $Mn_2SiO_4$ (0.46 %), and $Na_8Al_6Si_6O_{24}Cl_2$ (1.6 %).

Figure 8. Condensation temperatures of Fe metal, $Mg_2SiO_4$ forsterite, and $MgSiO_3$ enstatite in a solar composition gas as a function of total pressure.

Figure 9. Percentage distribution of sulfur between different phases in a solar composition gas as a function of temperature for a total pressure of $10^{-4}$ bars. Gaseous species are indicated with (g), all other species are condensed phases.

Figure 10. Percentage distribution of phosphorus between different phases in a solar composition gas as a function of temperature for a total pressure of $10^{-4}$ bars. Gaseous species are indicated with (g), all other species are condensed phases. Hydroxyapatite ($Ca_5(PO_4)_3OH$) has an abundance of 70% of total P, but occurs only at 300 K (and lower), and is therefore not shown.

Figure 11. Percentage distribution of fluorine between different phases in a solar composition gas as a function of temperature for a total pressure of $10^{-4}$ bars. Gaseous species are indicated with (g), all other species are condensed phases.

Figure 12. Percentage distribution of chlorine between different phases in a solar composition gas as a function of temperature for a total pressure of $10^{-4}$ bars. Gaseous species are indicated with (g), all other species are condensed phases.

Figure 13. Percentage distribution of oxygen between different phases in a solar composition gas as a function of temperature for a total pressure of $10^{-4}$ bars. Gaseous species are indicated with (g), all other species are condensed phases. The minor solids include: $Al_2O_3$ (0.28 %), $Ca_2Mg_5Si_8O_{22}(OH)_2$ (4.15 %), $Ca_5(PO_4)_3(F,Cl,OH)$ (0.25 %), $Ca_3(PO_4)_2$ (0.17 %), $CaTiO_3$ (0.05 %), $Cr_2O_3$ (0.14 %), $FeCr_2O_4$ (0.15 %), $FeTiO_3$ (0.05 %), $KAlSi_3O_8$ (0.21 %), $KMg_3AlSi_3O_{10}(OH)_2$ (0.31 %), $MgAl_2O_4$ (0.40 %), $MgCr_2O_4$ (0.18 %), $Mg_3Si_4O_{10}(OH)_2$ (0.27 %), $Mn_2SiO_4$ (0.13 %), $Na_8Al_6Si_6O_{24}Cl_2$ (0.44 %), $TiO_2$ (0.03 %), $Ti_4O_7$ (0.03 %), VO (0.002 %), $V_2O_3$ (0.003 %), $ZnCr_2O_4$ (0.03 %).

Figure 14. Percentage distribution of carbon between CO and $CH_4$ in a solar composition gas as a function of temperature and pressure. The line shows where CO and $CH_4$ have equal abundances. Above the line, CO is more abundant, whereas below the line, $CH_4$ is more abundant.

Figure 15. Percentage distribution of nitrogen between $N_2$ and $NH_3$ in a solar composition gas as a function of temperature and pressure. The line shows where $N_2$ and $NH_3$ have equal abundances. Above the line, $N_2$ is more abundant, whereas below the line, $NH_3$ is more abundant.

Figure 16. Gas phase chemistry of hydrogen in a solar composition gas as a function of temperature at a total pressure of $10^{-4}$ bars. The abundances of the gases are shown in mole fractions.

Figure 17. Percentage distribution of hydrogen between different phases in a solar composition gas as a function of temperature for a total pressure of $10^{-4}$ bars. Gaseous species are indicated with (g). Solid phases ($Na_2Mg_3Al_2Si_8O_{22}(OH)_2$, $Ca_5(PO_4)_3OH$, $Ca_2Mg_5Si_8O_{22}(OH)_2$, $KMg_3AlSi_3O_{10}(OH)_2$, $Mg_3Si_4O_{10}(OH)_2$) are not shown, due to their low abundances ($< 1 \times 10^{-4}$ %).

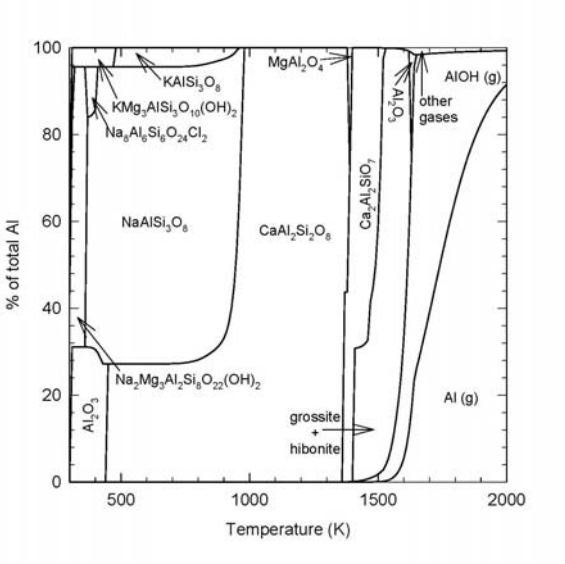


Figure 1.

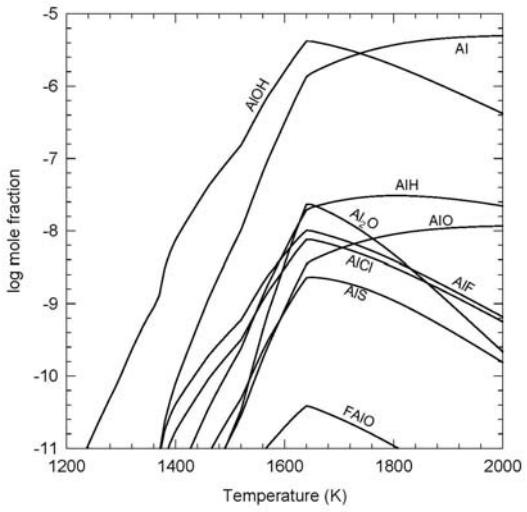


Figure 2.

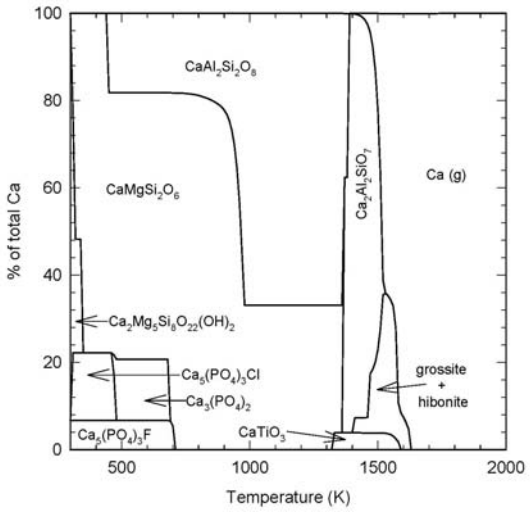


Figure 3.

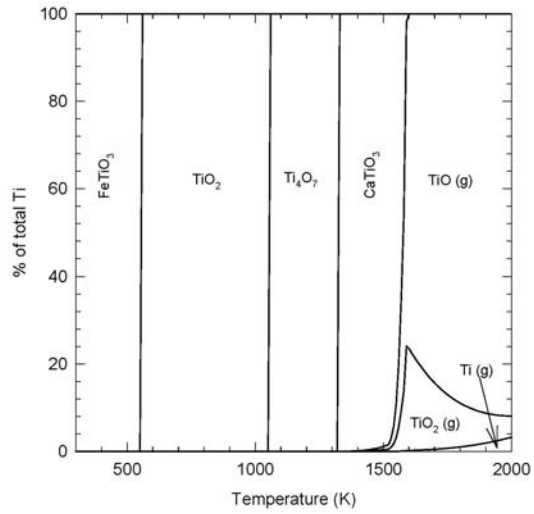


Figure 4.

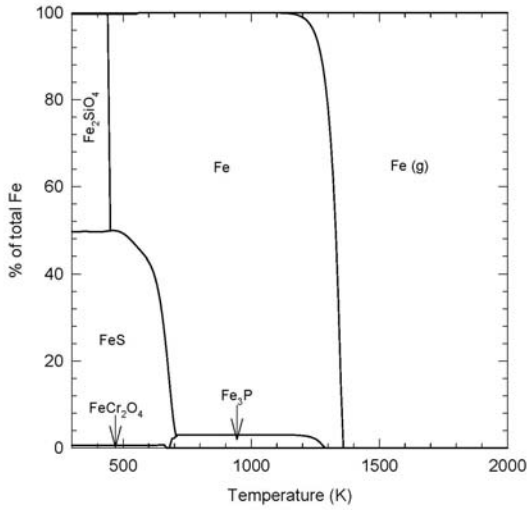


Figure 5.

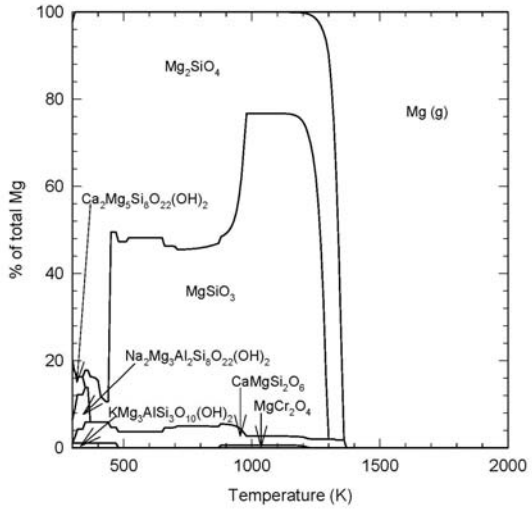


Figure 6

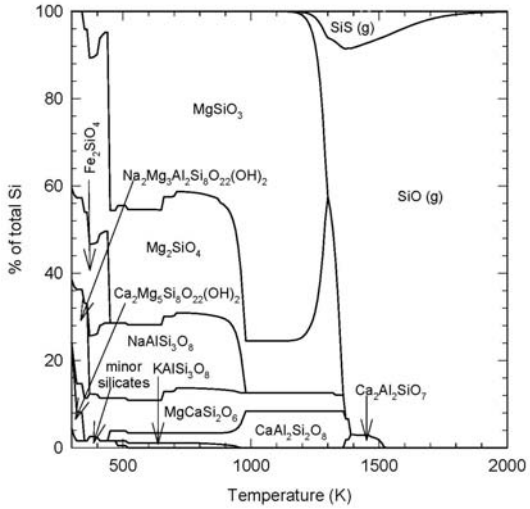


Figure 7.

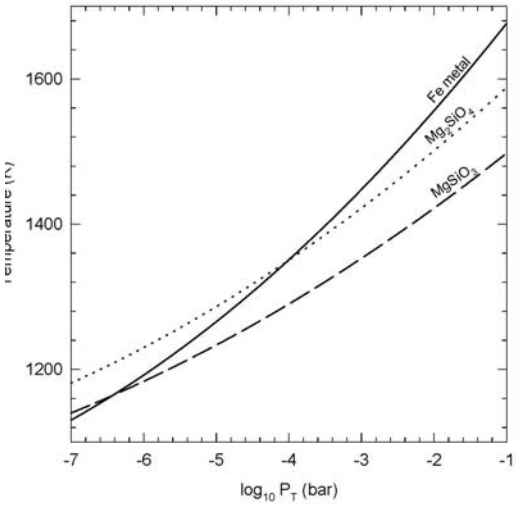


Figure 8

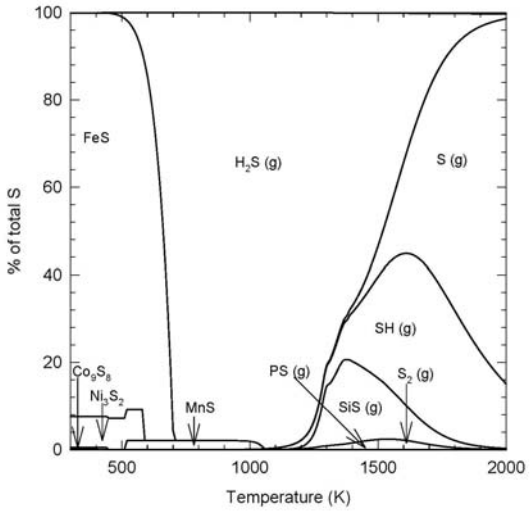


Figure 9

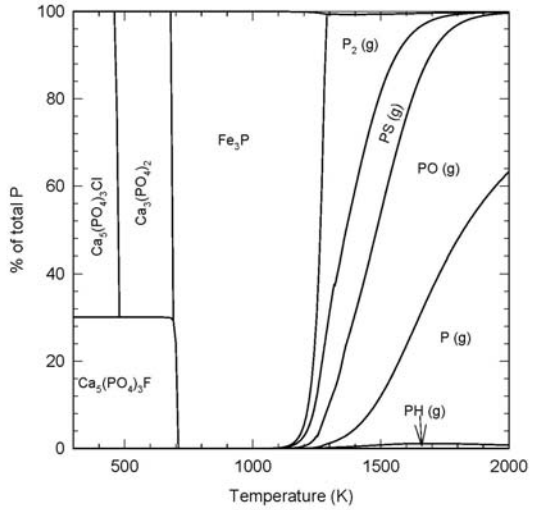


Figure 10

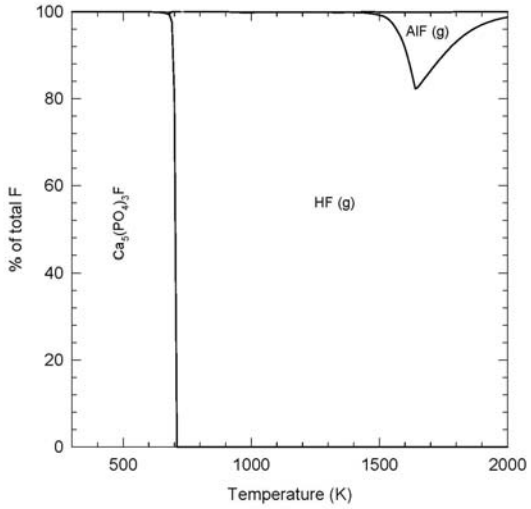


Figure 11

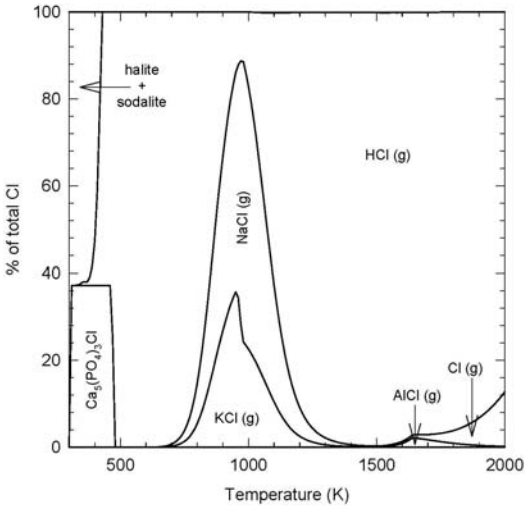


Figure 12

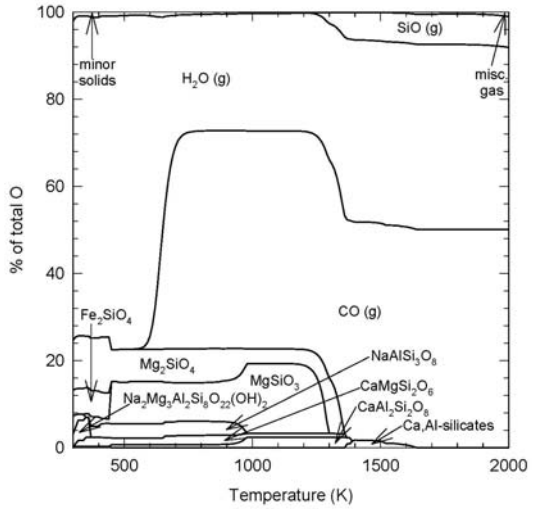


Figure 13

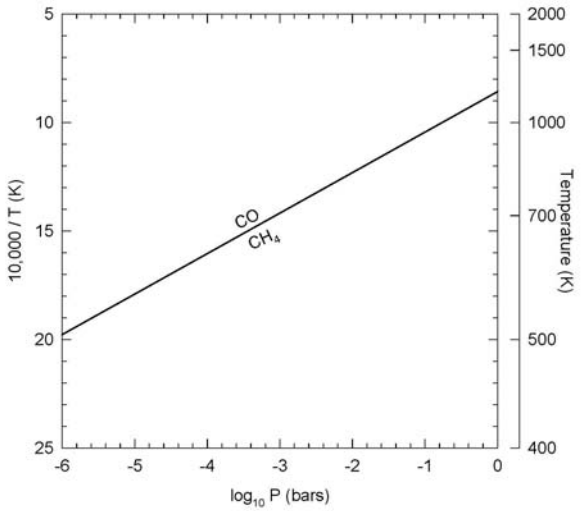


Figure 14

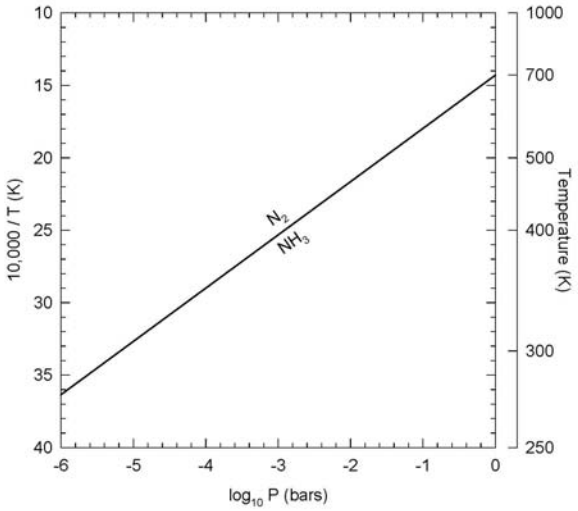


Figure 15

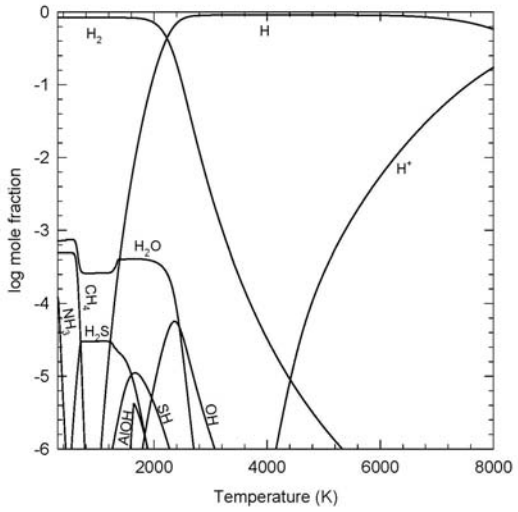


Figure 16

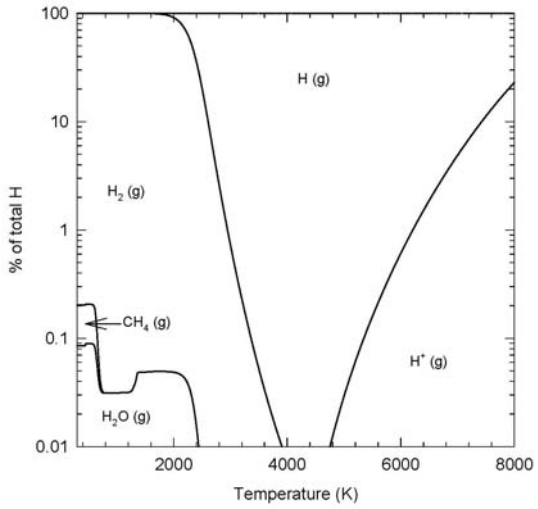
100
10
1
0.1
0.01
% of total H
H (g)
H$_2$ (g)
CH$_4$ (g)
H$_2$O (g)
H$^+$ (g)
2000
4000
6000
8000
Temperature (K)

Figure 17